A Novel Change Detection Technique for Occluded Objects using Ultra-Wideband Radar

Soumya Chakravarty*, Smriti Rani†, Arijit Chowdhury‡, Tapas Chakravarty§, Arpan Pal¶
TCS Research
Email : (*soumya.chakravarty1, †smriti.rani, ‡arijit.chowdhury2, §tapas.chakravarty, ¶arpan.pal) @tcs.com

***Abstract*—The burgeoning e-commerce business model has witnessed several cases where the packages with faulty goods, returned by the buyers, did not contain the procured object, rather being replaced by a different device. There is a need to unobtrusively detect any such changes in the content of the sealed package. In this paper, the penetrability of Ultra-Wideband (UWB) radar is utilized to build a change detection technique for making a quantitative assessment of the presence of an 8" Tab inside its sealed box, as opposed to other devices inside the same box. For this purpose, an electronic device is placed on an oscillating platform. A sliding Least-Of Constant False Alarm Rate (LO-CFAR) algorithm is applied on the radar scan data and the concept of detection sensitivity is introduced. Multiple experiments at different measurement instances are conducted to evaluate 1-class classification using detection sensitivity levels. These experiments show that the detection sensitivity levels provide a statistical basis for differentiating between objects. Also measurements were done at different distances, thus giving the result that the detection sensitivity level alone can be a determinant of the object type.**

***Index Terms*—UWB radar, CFAR, change detection, in-box imaging, detection sensitivity**

I. Introduction

The rapid expansion of the e-commerce market segment is largely triggered by the purchase of high-valued electronic consumer devices [1]. Majority of such devices like mobile phones, tablets, laptops, etc. are ordered online and delivered via couriers. This business model also encourages the buyer to return any faulty item. It is noted that in a few cases, the returned packages did not contain the procured object, instead being replaced by a different device or objects of other types. For such scenarios, the companies feel the need to check the content of the returned package without unsealing it. For this purpose, various technologies for imaging in occluded space are used, such as X Rays, Radio Frequency Identification (RFIDs), radars and several others [2], [3].

Among radars, Ultra-Wideband Radars (UWB) have demonstrated tremendous capability for through the wall imaging. For instance, Liang et al. [4] have used UWB technology for finding vital signs of a human seated behind a wall. Authors Song and his team have targeted building layout reconstruction using this revolutionary technology [5]. Pulsed UWB radars have high penetrability and superior resolution [4]. Thus, UWB technology can be used for scanning sealed packages. Unlike X Rays, they do not need specialised chambers for boxes to pass through. The radiated power levels from FCC/ETSI certified UWB is low enough to not cause harm to humans through exposure. Neither do they need RFID tags to be placed on the identifiable object. Portable UWB units reduce user hassle and thus can lead to large scale deployment of such units in warehouses [6], [7], [8].

Traditionally, moving target detection using radars in high interference environments has been done successfully using Constant False Alarm Rate (CFAR) algorithm and its various variants [9]. The CFAR algorithm takes every range bin from the radar data matrix and calculates the detection probability based on a computed threshold. Multiple variants of CFAR are found in literature, like cell averaging (CA), taking least of (LO-CFAR) of adjoining guard cells and reference cells, and others. LO-CFAR algorithm is often preferred due to its noise reduction capability caused by multi-path effects or background reflections. Recently, Akhtar et al. demonstrated a trained neural network [10] for object detection using CFAR algorithm. Additionally, CFAR algorithm suite has proved successful for noise estimation and detection using compressed sensing radar [11] as well.

Taking the industry use case, an end-to-end system including in-situ scanning on conveyer belts is envisaged. Towards this larger picture, a lab based Proof of Concept (PoC) is developed. A device is placed on a vibrating platform, which supports to and fro motion in lateral direction with respect to the look angle of the radar. A modified sliding CFAR detector algorithm is proposed, which is applied on the scan data from the radar, where the radar was kept static and the target objects were in to-and-fro motion. Object specific detection sensitivity is obtained, which is used as a differentiation factor among visually occluded devices. This is shown experimentally using an 8" tablet and a 6.4" mobile device, at different radial distances from the radar. Since the system is built using change detection of the material, shape and size using radar principles, it is generalizable across all possible devices with diverse make and models.

This paper is organised as follows. The overall system is explained in Section II. Section III outlines the process for threshold calculation for the LO-CFAR algorithm and method to ascertain the presence of the target based on this threshold. It is followed by experimental setup in Section IV and results and discussion in Section V. Paper is concluded in Section VI.

II. Overall System

For the purpose of the experiments, the PulsON 440 (P440) module, which is an UWB radio transceiver operating between

3.1 and 4.8 GHz in monostatic mode, is used. The antennas used in the radar unit are Time Domain's BroadSpec (planar elliptical dipole) antennas (beam pattern: Omnidirectional in azimuth to +/- 1.5dB) [12]. The configuration parameters of the radar module are controlled by the Graphical User Interface (GUI) called Monostatic Radar Module Reconfiguration and Evaluation Tool (MRM RET). Range resolution for the module is 0.0091 m. The configuration parameters are given in Table I.

TABLE I: THE CONFIGURATION PARAMETERS OF THE RADAR MODULE

Maximum Observable Range (m)	Pulse Integration Index (PII)	Transmit power delivered (dBm)	Scan Interval (ms)	No. of scans
$0.88 \times 2 = 1.66$ (2 quanta)	15	-31.6	125	300

In Fig. 1, the setup for the experiment is shown. The radar and target objects are surrounded by brick walls on three sides. Both the radar and the object are placed at approximately 1m height from the floor. The height at which the radar unit is placed is adjusted to align with the center of the target. The platform vibrates in the orthogonal plane to radar's look angle, i.e, in the direction of X-axis in Fig. 1a. The vibrating platform oscillates at a frequency of about 2.4 Hz.

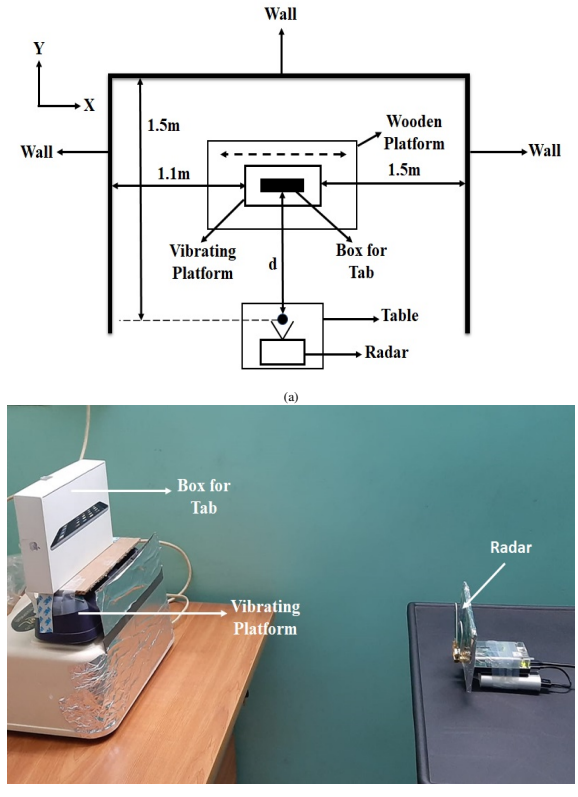

Fig. 1: The experimental setup: (a) Block diagram of the placement of the radar and the target object (b) Photograph showing both the object on vibrating platform and the UWB radar.

III. METHODOLOGY

Constant False Alarm Rate (CFAR) algorithm is typically used in radar applications for detection of moving objects, where radar is kept static since it offers robust detection mechanism. In this paper, specifically a sliding LO-CFAR (Least-Of-CFAR) algorithm is utilized to detect a high-value, linearly moving target object (to-and-fro motion in a plane orthogonal to the look angle of the radar) in an enclosed box and to determine if the contents of the box has been changed. The CFAR algorithm is shown in Fig. 2. The processes involved in this algorithm are described in the following subsections.

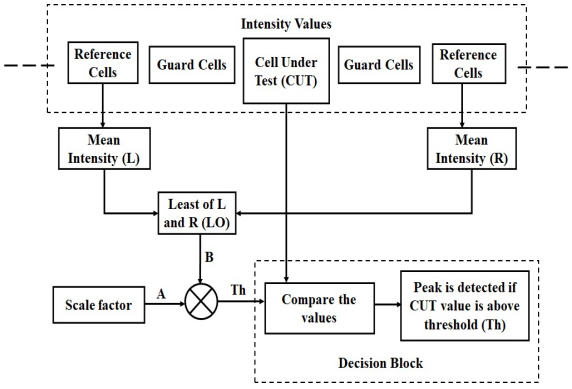

Fig. 2: Block diagram of LO-CFAR algorithm

A. Preprocessing

The back-scattered signal (obtained in the form of a range-time matrix from the radar unit) from the target is preprocessed in the given radar unit using a 3^{rd} order IIR (Infinite Impulse Response) bandpass filter covering 3.1-4.8 GHz. This data is subsequently motion-filtered using a 4-Tap difference filter, given by equation 1.

$$y(n) = x(n) - 0.6 \times x(n-1) - 0.3 \times x(n-2) - 0.1 \times x(n-3) \quad (1)$$

Lastly, a lowpass filter (6^{th} order IIR) is applied on the motion-filtered data to obtain its envelop. The above filters are the standard filters where the filter coefficients are configured as suggested by the manufacturer, Time Domain, for their PulsON 440 (P440) UWB radar module. The final dataset (range-time matrix) obtained after filtering is named as "M", which is an i×j matrix where i denotes the total number of scans and j denotes the total number of range bins from where the back-scattered signal is captured.

B. Threshold Calculation

The sliding CFAR algorithm is applied on "M" for every range bin and each scan time, to ascertain the presence of the desired target based on whether the intensity of the reflected signal exceeds a certain threshold value. The guard cells (each representing a range bin) immediately adjacent to every cell under test (CUT) are excluded from the calculation to avoid corrupting the estimate of the surrounding noise floor level

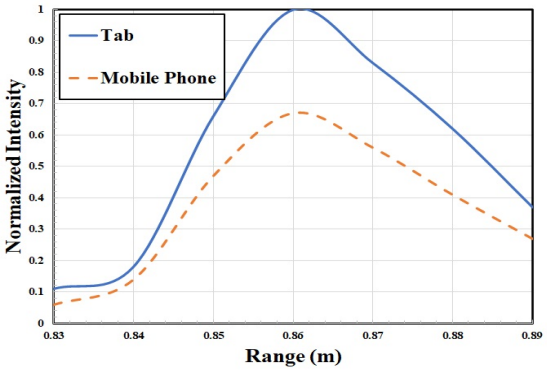

Fig. 3: Peak intensity of reflected signal from target objects at 0.75m from radar (normalized to Tab box)

with reflected power (I) from the target itself. The minimum (LO) of the averages of the reference cells present on both sides of the CUT, as obtained by the process described in Fig. 2, is then multiplied by a scale factor (α) to find the threshold. The scale factor is chosen based on a desired probability of false alarm, so that the ratio of correct and false detections can be set. False alarm occurs when the intensity of the reflected signal exceeds the threshold at a time and range point where no target is actually located. This leads to a false detection of a target, thus decreasing the accuracy of the measurement. The scale factor, as given in [13], is calculated as shown in equation 2:

$$\alpha = N.(P_n^{-1/N} - 1) \tag{2}$$

where, N is the total number of reference cells (here, 40) and P_n is the probability of false alarm (here, 0.001). With α and LO being computed, the threshold value (Th) is now calculated by simply multiplying the two values. The detections are made based on the following relations as given in [14].

$$\begin{cases} I_{CUT} \geq Th & \Rightarrow H_{CUT} = 1\text{: target detected} \\ I_{CUT} \leq Th & \Rightarrow H_{CUT} = 0\text{: no target} \end{cases} \tag{3}$$

where, I_{CUT} is the intensity value of the back-scattered signal at the position of the CUT and H_{CUT} is the value at the position of the CUT in the matrix obtained after applying CFAR on "M".

C. Object-specific detection sensitivity

The target objects with the box have a non-negligible width (4cm) which results in a band of detections in the CFAR matrix starting from the location of front edge of the target and ending at some distance beyond. Thus, further evaluations are restricted in a window of range bins around the object's position. This is termed as range gate which is given as:

$$\Delta R = R_2 - R_1, \quad (R_1 < d < R_1)$$

where, R_1 and R_2 are the lower and upper bounds of the range gate, respectively. For the present case, it is considered that ΔR = 20cm.

As described in Section III-B, initially, the threshold for detection is determined with "α" being calculated as stated in equation 2. This is denoted as "α_{min}". Then, the value of "α" is increased, till the detection sensitivity level is reached. When the moving object is detected by using the default scale factor, the area under the curve (AUC) between R_1 and R_2 is computed over the entire scan time. This is essentially equivalent to counting the number of '1's (or number of cells for which object is detected), which is expressed as:

$$AUC(\alpha_{min}) = \sum_{t=0}^{t_1} \sum_{R_1}^{R_2} H_{CUT} \tag{4}$$

Using this, detection sensitivity (S) is calculated. As α is increased, AUC(α_{min}) decreases. Detection sensitivity is defined as the value of scale factor that results in the number of detections in the CFAR matrix falling to a certain critical level, below which it can be decided that the desired object is not present. Value of "S" is obtained when the following condition is fulfilled:

$$AUC(S) = k.AUC(\alpha_{min}) \tag{5}$$

where,

$$0 < k \leq 1$$

The variation in the value of 'k' results in different levels of measurement precision. $k = 0.1$ is applied for the presented results. Now, the factor "k" is configurable and can be adjusted so that the measurement repeatability is ensured. When a higher value of "k" is given (e.g., $k = 0.3$), the sensitivity level gets reduced and vice-versa. At low sensitivity levels, the percentage variation in "S" is expected to be small for multiple instances of measurement. However, the purpose of this change detection method is then lost since there is every likelihood that the sensitivity levels for objects with similar sizes and shapes will be identical or with variations small enough to not be inferred as two distinct objects. Therefore, in real deployment scenarios, the "k" value needs to be suitably adjusted with initial training cycle.

IV. Experimental Paradigm

Multiple investigations are conducted to distinguish between the desired target, being an 8" inch Tab (e.g., iPad Mini) in a sealed box, versus other non-Tab objects like an empty Tab box, the box with 6.4" mobile phone and box with eBook Paperwhite (Kindle). The different objects have different reflection and absorption characteristics, thus providing a basis for detecting significant change in the content of the box. Measurements are taken for the box to investigate the variability of detection sensitivity levels at a given distance. Also, for each object, measurements are taken at four distances of separation between radar and target, which is indicated by "d" (in Fig. 1a) where, d = 0.75m, 0.85m, 0.95m, 1.05m.

V. Results and Discussion

From the experiments described above, the back-scattered signal for the two cases, namely 6.4" mobile phone and 8" Tab in box, are plotted in Fig. 3, which displays the peak intensity values and the corresponding ranges. The Tab box has a depth

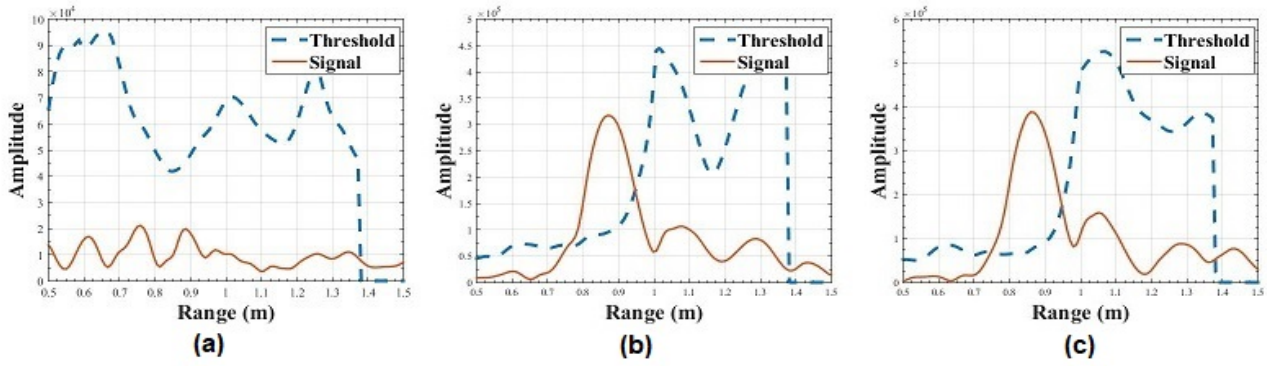

Fig. 4: Threshold values and intensity of reflected signal for all ranges for (a) the empty Tab box, (b) the 6.4" mobile phone inside the box and (c) the Tab inside the box at 10s time point at d = 0.75m

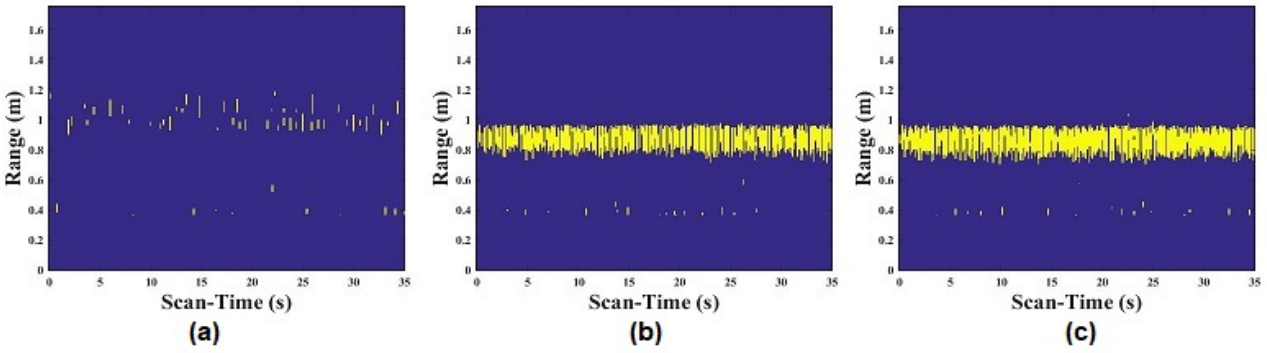

Fig. 5: CFAR images at alpha = 7.54 and d = 0.75m for (a) empty Tab box, (b) the same box containing mobile phone and (c) the same box containing Tab

of 4 cm which corresponds to approximately 4 range bins from the entry and exit points. However, from the plots, it is noticed that there is a spread of received signal over 10 cm in range. This is partly accounted for by the averaging process induced by 4-Tap difference filter followed by 6^{th} order low pass filter.

At the same time, it is to be noted that the box, by default, consists of the charger and other packaging materials, which leads to the possibility that the speed of electromagnetic wave is reduced (due to higher dielectric constant), thus resulting in range-stretching.

In the next step, the threshold values for all the range bins are computed. Fig. 4 displays the threshold values and the signal intensity at a distance of 0.75 m and for a given instance of time for all the three objects, namely the empty Tab box, the 6.4" mobile phone and the 8" Tab. From Fig. 4, it is observed that the detection range (represented by the peak of the amplitude curve of the signal) is followed by a sharp increase in the threshold value at a nominally fixed distance from the target and behind the target with respect to the radar. This effect (named here as "shadow" region) is consistent for both Tab and mobile phone for all the four measurement distances. The shadow is observed to be formed in between 0.14m to 0.18m distance behind the object.

Initially, the scale factors (pt. A in Fig. 2) are computed as described in Section III-B, giving a result of α_{min} = 7.54. Using this default scale factor, the CFAR images of all the objects for a measurement distance of 0.75 m are plotted in the range-time scale. This is displayed in Fig. 5.

Any radar measurement is critically dependent on the measurement setup as well as the environment. Variations in detection sensitivity level for the same Tab inside box is anticipated for different measurement instances. To test the variability, ten measurements are taken at different instances of time. In Fig. 6, the percentage variation of the values of "S" for the Tab at a distance of 0.95m is displayed for k = 0.01 and 0.1 respectively. The measurement parameters are kept

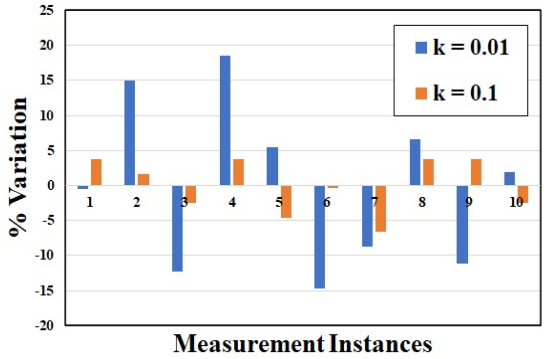

Fig. 6: Percentage Variation of detection sensitivity for tablet in box at different measurement instances at 0.95m

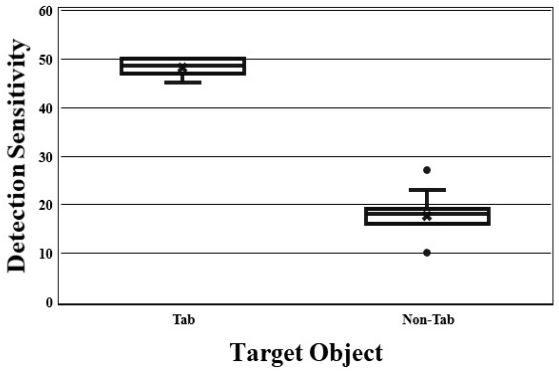

Fig. 7: Box Plot for Detection Sensitivity Values for Tab and Non-Tab cases

identical in all instances and the measurements are taken by putting the object in the radar's line-of-sight and pulling it out immediately after a fixed scan time period. The percentages are calculated with respect to the mean value of "S" obtained from all the ten observations.

The results presented in Fig. 6 validate the hypothesis discussed in Section III-C that by setting $k = 0.01$, wider variation of detection sensitivity levels for the same object will be obtained. For the change detection to take place, the "sensitivity band" needs to be ideally unique for the desired Tab. In a real deployment scenario, the "sensitivity band" needs to be learnt in the initial training cycle and a machine-learning based 1-class classification can be applied.

The detection sensitivity values, at a fixed distance of 0.95m, for both Tab and non-Tab categories are shown in Fig. 7. It is observed that the distributions are statistically separated and thus can be easily differentiated. Hence, it is possible to apply learning algorithms in a different scenario, if need be.

The detection sensitivity levels for the Tab and mobile phone are further evaluated at four measurement distances. These detection sensitivity ratios for the Tab to empty box and that of Tab to mobile phone are tabulated in Table II.

TABLE II: RATIOS OF DETECTION SENSITIVITY FOR FOUR MEASUREMENT DISTANCES (D) OF THE TARGETS

d (m)	Detection Sensitivity ratios	
	$(S_{Tab}/S_{emptybox})$	(S_{Tab}/S_{mobile})
0.75	4.95	1.41
0.85	4.36	1.26
0.95	4.69	1.36
1.05	5.03	1.42

From Table II, it is observed that the ratios of detection sensitivities are distinctly different for all three cases. This observation illustrates that:

a) the presence of a 8" Tab vs a 6.4" mobile phone inside the box is easily identifiable when the object is in motion with respect to the radar.
b) "S" is the sole determinant for identification of the type of the object inside the box, thus offering a successful approach for change detection.

VI. CONCLUSION

The process of identifying distinct features of a primarily non-metallic object is difficult in an RF-dense environment due to the high levels of static clutter signal. In this paper, a novel UWB radar-based change detection technique is introduced where the radar is static and target is in to-and-fro motion. The purpose of the study is to establish a quantitative method to distinguish a high-value consumer product (e.g., a concealed iPad) from other similar devices. Towards this objective, a sliding CFAR algorithm is used to compute the detection sensitivity levels. Here, the scale factor in the CFAR algorithm is adapted to obtain the detection sensitivity thresholds for each object. It is shown that these detection sensitivity levels for Tab and non-Tab objects (where both are inside the identified box) are statistically separated, thereby offering an easy method to detect a change inside the package through comparative analysis.

REFERENCES

[1] S. Chava, A. Oettl, M. Singh, and L. Zeng, "Impact of e-commerce on employees at brick-and-mortar retailers," *Economics of Innovation eJournal*, 2018.
[2] S. Seol, E.-K. Lee, and W. Kim, "Indoor mobile object tracking using rfid," *Future Generation Computer Systems*, vol. 76, pp. 443–451, 2017.
[3] D. Oloumi and K. Rambabu, "Metal-cased oil well inspection using near-field uwb radar imaging," *IEEE Transactions on Geoscience and Remote Sensing*, vol. 56, no. 10, pp. 5884–5892, 2018.
[4] F. Liang, M. Liu, F. G. Qi, H. Lv, H. J. Xue, G. Lu, and J. Wang, "Through the wall imaging of human vital signs based on uwb mimo bioradar," *Progress In Electromagnetics Research*, vol. 87, pp. 119–133, 2018.
[5] Y. Song, J. Hu, N. Chu, T. Jin, J. Zhang, and Z. Zhou, "Building layout reconstruction in concealed human target sensing via uwb mimo through-wall imaging radar," *IEEE Geoscience and Remote Sensing Letters*, vol. 15, no. 8, pp. 1199–1203, 2018.
[6] B. Y. Kapilevich, S. W. Harmer, and N. J. Bowring, *Non-imaging microwave and millimetre-wave sensors for concealed object detection*. CRC Press, 2014.
[7] T. Liu, Y. Zhao, Y. Wei, Y. Zhao, and S. Wei, "Concealed object detection for activate millimeter wave image," *IEEE Transactions on Industrial Electronics*, vol. 66, no. 12, pp. 9909–9917, 2019.
[8] K. Yu, X. Qi, T. Sato, Z. Wen, Y. Katsuyama, K. Tokuda, W. Kameyama, T. Sato *et al.*, "Design and performance evaluation of an ai-based w-band suspicious object detection system for moving persons in the iot paradigm," *IEEE Access*, vol. 8, pp. 81 378–81 393, 2020.
[9] M. A. Richards, *Fundamentals of radar signal processing*. McGraw-Hill Education, 2014.
[10] J. Akhtar, "Training of neural network target detectors mentored by so-cfar," in *2020 28th European Signal Processing Conference (EUSIPCO)*. IEEE, 2021, pp. 1522–1526.
[11] D. Kozlov and P. Ott, "Cfar detector for compressed sensing radar based on l 1-norm minimisation," in *2020 28th European Signal Processing Conference (EUSIPCO)*. IEEE, 2021, pp. 2050–2054.
[12] A. Chowdhury, T. Das, S. Rani, A. Khasnobish, and T. Chakravarty, "Activity recognition using ultra wide band range-time scan," in *2020 28th European Signal Processing Conference (EUSIPCO)*. IEEE, 2021, pp. 1338–1342.
[13] G. M. Hatem, J. A. Sadah, and T. R. Saeed, "Comparative study of various cfar algorithms for non-homogenous environments," in *IOP Conference Series: Materials Science and Engineering*, vol. 433, no. 1. IOP Publishing, 2018, p. 012080.
[14] J. Pan, S. Ye, C. Shi, K. Yan, X. Liu, Z. Ni, G. Yang, and G. Fang, "3d imaging of moving targets for ultra-wideband mimo through-wall radar system," *IET Radar, Sonar & Navigation*, 2021.